Rational Design of Intrinsically Ultramicroporous Polyimides Containing Bridgehead-Substituted Triptycene for Highly Selective and Permeable Gas Separation Membranes

ARTICLE *in* MACROMOLECULES · JULY 2014

Impact Factor: 5.8 · DOI: 10.1021/ma5009226

5 AUTHORS, INCLUDING:

Raja Swaidan
Air Liquide America
18 PUBLICATIONS **337** CITATIONS
SEE PROFILE

Bader Ghanem
King Abdullah University of Science and Techn…
38 PUBLICATIONS **2,041** CITATIONS
SEE PROFILE

Macromolecules

Article

pubs.acs.org/Macromolecules

Rational Design of Intrinsically Ultramicroporous Polyimides Containing Bridgehead-Substituted Triptycene for Highly Selective and Permeable Gas Separation Membranes

Raja Swaidan,[†] Majed Al-Saeedi,[‡] Bader Ghanem,[†] Eric Litwiller,[†] and Ingo Pinnau*[,†]

[†]Advanced Membranes and Porous Materials Center (AMPMC), Physical Sciences and Engineering Division, King Abdullah University of Science and Technology, Thuwal 23955-6900, KSA

[‡]Department of Chemistry, Taibah University, Madinah 30001, KSA

Supporting Information

ABSTRACT: Highly ultramicroporous, solution-processable polyimides bearing 9,10-bridgehead-substituted triptycene demonstrated the highest BET surface area reported for polyimides (840 m^2 g^{-1}) and several new highs in gas selectivity and permeability for hydrogen (1630−3980 barrers, H_2/CH_4 ∼ 38) and air (230−630 barrers, O_2/N_2 = 5.5−5.9) separations. Two new dianhydrides bearing 9,10-diethyl- and 9,10-dipropyltriptycenes indicate that the ultramicroporosity is optimized for fast polymeric sieving with the use of short, bulky isopropyl bridgeheads and methyl-substituted diamines (TrMPD, TMPD, and TMBZ) that increase intrachain rigidity. Mechanically, the triptycene-based analogue of a spirobisindane-based polyimide exhibited 50% increases in both tensile strength at break (94 MPa) and elastic modulus (2460 MPa) with corresponding 90% lower elongations at break (6%) likely due to the ability of highly entangled spiro-based chains to unwind. To guide future polyimide design, structure/property relationships are suggested between the geometry of the contortion center, the diamine and bridgehead substituent, and the mechanical, microstructural, and gas transport properties.

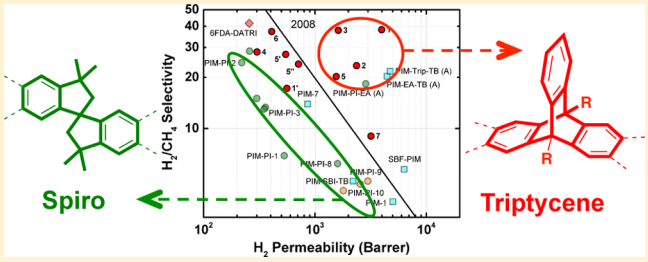

INTRODUCTION

The potential of membrane technology to offer simple, energy-efficient, and sustainable solutions to key industrial separations has sparked strong research efforts in material design and development.[1,2] High free-volume polymers of intrinsic microporosity (PIMs) are at the crux of a vibrant pursuit for advanced gas storage,[3−5] low-*K* dielectric,[6] and membrane-based gas separation[7−25] materials. Via integration of sites of contortion into rigid macromolecular architectures, intersegmental packing and intrasegmental mobility can be simultaneously inhibited in PIMs such that the microporosity (<20 Å) and high surface areas of inorganic materials are combined with the solution processability and structural tunability of amorphous polymers.[26] To date, a spiro-center—i.e., single tetrahedral carbon atom shared by two rings—has facilitated the design and synthesis of solution-processable ladder-type PIMs[7,10,27] and PIM-polyimides (PIM-PIs)[12,13,21,23] that were cast into self-standing membranes with surface areas exceeding 800 m^2 g^{-1} and significantly higher gas permeabilities than conventional, low-free-volume polymers including commercial materials like Matrimid and cellulose acetate. Notable improvements in the surface areas and selectivities of ladder PIMs as well as the permeabilities *and* selectivities of the PIM-PIs were achieved by replacement of the relatively flexible[28] spiro-centers with bulky, torsion-resistant bridged bicyclics: i.e., (i) ethanoanthracene,[8] unsubstituted triptycene,[9] and Tröger's base[8,9] moieties for the ladder PIMs and (ii) ethanoanthracene[24] and 9,10-diisopropyl-substituted triptycene[22] moieties for the PIM-PIs. This has driven the resulting gas separation performance over the latest state-of-the-art permeability/selectivity trade-off curves[29] for various gas pairs central to key industrial separations, namely O_2/N_2, H_2/CH_4, and H_2/N_2. In particular, significant enhancements in selectivity were reported for the polymers kinked by bridged bicyclics including triptycene and ethanoanthracene. Qualitative microstructural investigations of pore-size distributions in the polyimides using physisorption experiments indicated the development of a more pronounced sieving ultramicroporosity (<7 Å) attributed to a more inefficient packing of rigidified backbones.[22]

The above-mentioned studies emphasize the impact of the shape (i.e., kink angle), rigidity (i.e., shape persistence), and three-dimensional character of the contortion site on the macromolecular rigidity, pore-size distributions, and ultimately the resulting gas transport properties of the solution-cast polymer microstructures.[19] Here, we expand on our preliminary data[22] presented for KAUST-PI-1 and KAUST-PI-2, two 9,10-diisopropyl-triptycene-based PIM-PIs exhibiting high permeabilities and exceptional molecular sieving, with a wider set of

Received: May 5, 2014
Revised: July 2, 2014
Published: July 15, 2014

   dx.doi.org/10.1021/ma5009226 | *Macromolecules* 2014, 47, 5104−5114

Scheme 1. Triptycene-Based PIM-PIs Prepared with Various Alkyl Bridgehead Substituents (R = *i*-C_3, *n*-C_3, and C_2) and Commercially Available Diamines

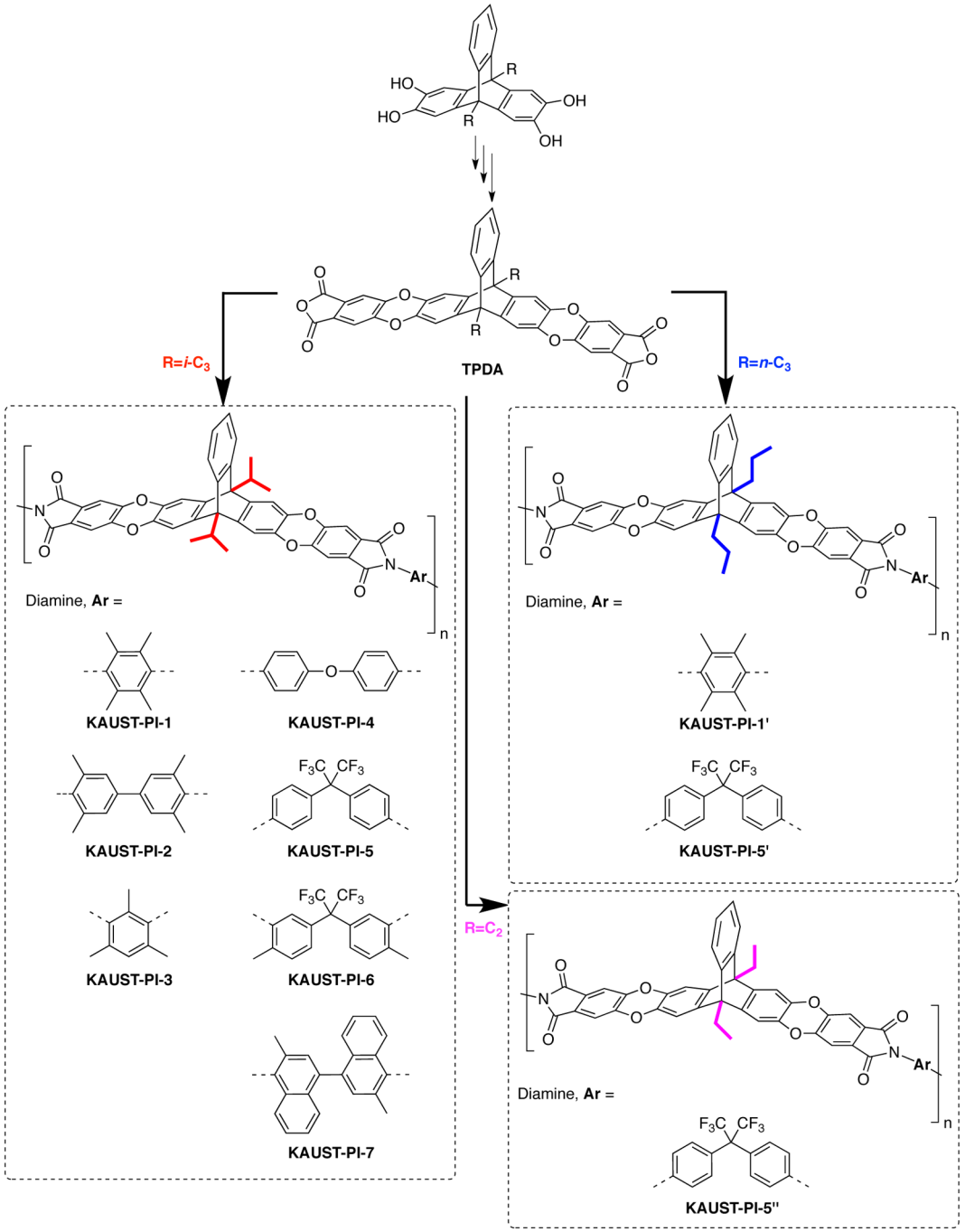

diamines to establish more extensive structure–property relationships that elucidate the effect of the triptycene moiety on tuning the gas transport and mechanical properties of PIM-PIs. In addition, the effect of the 9,10-bridgehead substituents (branched or linear alkyl chains) is investigated through physisorption and gas permeation studies on two new dianhydrides (bearing 9,10-diethyl- and 9,10-dipropyl-substituted triptycenes) reacted with different aromatic diamines (TMPD and 6FpDA). Full details of the synthesis and characterization of all the monomers and polymers are provided as well as the pure-gas transport properties for He, H_2, N_2, O_2, CH_4, and CO_2 at 2 bar and 35 °C. Data from the literature are analyzed in conjunction with that determined in this work to suggest a general set of recommendations guiding the design of more permeable *and* selective and mechanically robust PIM-PIs.

EXPERIMENTAL SECTION

Materials. The compounds 1,2-dimethoxybenzene, propanal, butanal, 2-methylpropanal, 2-aminobenzoic acid, (3-methylbutyl) nitrite, boron tribromide (BBr_3), 4,5-dichlorophthalonitrile, potassium hydroxide (KOH, Aldrich), acetic anhydride, isoquinoline, potassium carbonate (K_2CO_3), anhydrous dimethylformamide (DMF), 2,3,5,6-tetramethyl-1,4-phenylenediamine (TMPD), 3,3′,5,5′-tetramethylbenzidine (TMBZ), 5,5′-(hexafluoroisopropylidene)-di-*o*-toluidine (ATAF), 4,4′-oxidianiline (*p*,*p*′-ODA), and 4,4′-(hexafluoroisopropylidene)dianiline (6FpDA) were used as received.

dx.doi.org/10.1021/ma5009226 | *Macromolecules* 2014, 47, 5104–5114

2,4,6-Trimethyl-1,3-phenylenediamine (TrMPD) and 3,3′-dimethylnaphthidine (DMN) were purified by sublimation under vacuum. *m*-Cresol was distilled under reduced pressure and stored under nitrogen in the dark over 4 Å molecular sieves. All other solvents were obtained from various commercial sources and used as received.

Structural Characterization Methods. Flash chromatography was performed on silica gel 60A (35−70 μm, Fisher Scientific). ^{1}H NMR (400 MHz) and ^{13}C NMR (100 MHz) spectra were recorded on a Bruker DRX 400 spectrometer in a suitable solvent using trimethylsilane as the internal standard. Chemical shifts (δ) are reported in ppm. Column chromatography was performed on silica gel 60A. Fourier transform infrared (FT-IR) measurements were performed using a Varian 670-IR FT-IR spectrometer. Gel permeation chromatography (GPC, Viscotek) analyses were carried out using chloroform as an eluent. Thermogravimetric analysis (TGA, TA Q-5000) measurements were carried out under a nitrogen atmosphere. All analyses entailed a drying step at 100 °C for 30 min followed by a ramp of 3 °C/min to 800 °C. Mechanical properties were obtained with a DMA (TA Q800) using dog-bone specimens. The BET surface area of the polymers was measured with N_2 sorption at 77 K using a Micromeritics ASAP-2020. Powder polymer samples were degassed under high vacuum at 120 °C for 15 h prior to analysis. Analysis of the pore-size distributions was performed using the NLDFT (non-local density functional theory) model for carbon slit pore geometry provided by ASAP 2020 version 4.02 software.

Synthesis of Ethyl-Based Dianhydride Monomer (C_2 TPDA). The synthetic procedure for the ethyl-based dianhydride (C_2 TPDA) of Scheme 1 is similar to that previously reported for the isopropyl-based dianhydride.[22] First, 2,3,6,7-tetramethoxy-9,10-diethylanthracene was prepared by dropwise addition of a cooled mixture of 1,2-dimethoxybenzene (13.8 g, 0.1 mol), propanal (0.1 mol), and acetonitrile (5 mL) to a stirred solution of concentrated H_2SO_4 (50 mL) at 0−5 °C over 30 min. After stirring for 2 h at room temperature, the reaction mixture was quenched in 300 mL of ice-cold water. The precipitate was filtered, washed with water and methanol, and recrystallized from acetone to give the product as a white powder (20% yield, mp 232−234 °C). A diazonium salt was prepared by addition of concentrated HCl (3.6 mL), (3-methylbutyl) nitrite (8.6 mL), and diethyl ether (100 mL) to a stirred suspension of anthranilic acid (5.0 g, 36 mmol) in ice-cooled ethanol (100 mL), filtered, washed with ether, dried, and then added to a stirred solution of 2,3,6,7-tetramethoxy-9,10-diethylanthracene (5 mmol) in dichloroethane (60 mL) and 1,2-epoxypropane (5 mL). After 4 h of reflux under a N_2 atmosphere, the solvent was removed under vacuum, and the residue was purified by column chromatography over silica gel with dichloromethane (DCM)/ethyl acetate 99:1 as an eluent and recrystallized from ethanol/water to yield 2,3,6,7-tetramethoxy-9,10-diethyltriptycene (92% yield, mp 157−158 °C). The product was reacted with BBr_3, filtered, washed, and recrystallized from ethyl acetate/petroleum ether to yield the tetrahydroxy analogue (95% yield), which was reacted (1.9 mmol) with 4,5-dichlorophthalonitrile (3.7 mmol) in the presence of K_2CO_3 (7.4 mmol) in anhydrous DMF (15 mL) to yield the bisphthalonitrile as a white solid (72% yield). A solution of KOH (4.7 mmol in 12 mL of water) was added to a suspension of the bisphthalonitrile (2.4 mmol) in ethanol (12 mL), and the mixture was refluxed for 10 h. The filtrate was acidified, separated, and dried in a vacuum oven at 60 °C to give the tetracarboxylic acid as a light brown solid (99% yield). ^{1}H NMR (400 MHz, DMSO-d_6, δ): 1.33 (t, 6H, J = 6.4 Hz), 2.35 (q, 4H), 6.69 (s, 4H), 6.90 (m, 2H), 7.09 (s, 4H), 7.20 (m, 2H). ^{13}C NMR (100 MHz, DMSO-d_6, δ): 10.4, 18.7, 52.5, 111.2, 117.2, 122.1, 124.7, 129.7, 136.9, 142.5, 143.1, 167.0, FT-IR (KBr disk, cm^{-1}): 3375 (carboxylic CO−H stretching), 3064 (aromatic C−H), 2945 (aliphatic C−H), 1716 (C═O, str), 1224 (C−O−C str).

The tetracarboxylic acid (1.8 mmol) was added to acetic anhydride (10 mL) with heating and reflux under Ar for 12 h, after which cooling to 80 °C yielded a yellow precipitate collected by filtration and washed with acetic acid and toluene and dried to give the dianhydride C_2 TPDA (90% yield). Elem. Anal. Calcd (%) for $C_{40}H_{22}N_4O_{10}$: C, 72.51; H, 3.35. Found: C, 70.78; H, 3.49. ^{1}H NMR (400 MHz, $CDCl_3$, δ): 1.68 (t, 6H, J = 7.2 Hz), 2.88 (q, 4H, J = 6.8 Hz), 6.95 (s, 4H), 7.08 (m, 2H), 7.28 (s, 4H), 7.37 (m, 2H). ^{13}C NMR (100 MHz, $CDCl_3$, δ): 10.6, 19.7, 52.9, 111.6, 113.2, 122.1, 125.1, 127.4, 136.9, 148.9, 161.7. FT-IR (KBr disk, cm^{-1}): 3049 (aromatic C−H), 2937 (aliphatic C−H), 1851 (asym C═O), 1780 (sym C═O), 1215 (C−O−C str). HRMS (ESI): calcd for $C_{40}H_{22}O_{10}$ [M]$^+$: 662.12. Found 662.119.

Synthesis of Propyl-Based Dianhydride Monomer (*n*-C_3 TPDA). Following the same procedure for C_2 TPDA except starting with butanal as an aldehyde in the synthesis of the anthracene (22% yield, mp 235−236 °C), dianhydride *n*-C_3 TPDA (Scheme 1) was obtained as a yellow solid (86% yield, mp > 300 °C). ^{1}H NMR (400 MHz, $CDCl_3$) δ (ppm): 1.41 (t, 6H, J = 7.2 Hz), 2.41 (m, 4H), 2.75 (t, 4H, J = 7.2), 6.93 (s, 4H), 7.07 (dd, 2H, J = 2.3 Hz), 7.3 (s, 4H), 7.37 (m, 2H). ^{13}C NMR (400 MHz, $CDCl_3$) δ (ppm): 15.9, 18.4, 30.5, 30.9, 52.4, 111.5, 113.2, 122.1, 125.2, 127.4, 136.9, 148.9, 161.7, 207.0. FT-IR: 3020 (aromatic C−H), 2921 (aliphatic C−H), 1840 (asym C═O), 1776 (asym sym C═O).

Synthesis of Isopropyl-Based Dianhydride Monomer (*i*-C_3 TPDA). Following the same procedure for C_2 TPDA except starting with 2-methylpropanal in the synthesis of the anthracene, the dianhydride *i*-C_3 TPDA was obtained as a yellow solid (84% yield).[22] Elem. Anal. Calcd (%) for $C_{42}H_{26}O_{10}$: C, 73.04; H, 3.79. Found: C, 72.44; H, 3.53. ^{1}H NMR (400 MHz, $CDCl_3$, δ): 1.77−1.91 (m, 12H), 3.31−3.50 (m, 4H), 6.96−7.86 (m, 12H). FT-IR (powder, ν, cm^{-1}): 3020 (aromatic C−H), 2921 (aliphatic C−H), 1840 (asym C═O), 1776 (sym C═O). HRMS (ESI): calcd for $C_{42}H_{26}O_{10}$ [M]$^+$: 690.15; Found 690.15.

Typical Procedure for the Synthesis of KAUST-PIs. To a dry 25 mL reaction tube equipped with a Dean−Stark trap with a nitrogen inlet were added the diamine (1.0 mmol) and freshly distilled *m*-cresol (7 mL). The mixture was stirred at room temperature for 5 min. An equimolar amount of dianhydride monomer (1.0 mmol) and isoquinoline (0.1 mL) were added. The reaction mixture was stirred at room temperature for 1 h, and the temperature was raised gradually to 200 °C and held for 4 h under a nitrogen atmosphere. During this period the water formed by the imidization reaction was removed by azeotropic distillation using anhydrous toluene. After cooling to room temperature, fibrous polyimide was obtained by the dropwise addition of the polymer solution to methanol. The resulting solid was filtered, purified by reprecipitation from chloroform into methanol, and then dried at 120 °C in a vacuum oven for 20 h.

The characterizations for KAUST-PI-1 and KAUST-PI-2 have been recently reported.[22]

KAUST-PI-1′. Following the above general procedure, KAUST-PI-1′ was prepared from the dianhydride *n*-C_3 TPDA and TMPD diamine as an off-white powder (90% yield). ^{1}H NMR (400 MHz, $CDCl_3$, δ): 1.24 (br m, 6H), 2.00 (br s, 12H), 2.15 (br m, 4H), 2.7 (br m, 4H), 6.94 (br s, 4H); 7.07 (br m, 2H); 7.30 (br s, 4H); 7.37 (br m, 2H). FT-IR (KBr, cm^{-1}): 1780 (asym C═O, str), 1726 (sym C═O, str), 1356 (C−N, str), 744 (imide ring deformation). GPC ($CHCl_3$): M_n = 48 000 g mol^{-1}, M_w = 72 000 g mol^{-1} relative to polystyrene, M_w/M_n = 1.5. BET surface area = 610 m^2 g^{-1}, total pore volume = 0.44 cm^3 g^{-1} at (p/p_0 = 0.98, adsorption). TGA analysis: (nitrogen), thermal degradation commences at T_d ~ 415 °C.

KAUST-PI-3. Following the above general procedure, KAUST-PI-3 was prepared from the dianhydride *i*-C_3 TPDA and TrMPD diamine as a pale-yellow powder (97% yield). ^{1}H NMR (400 MHz, $CDCl_3$, δ): 1.88 (br m, 15H), 2.17 (br s, 6H), 3.3−3.49 (br m, 2H), 6.93−7.79 (br m, 13H). FT-IR (membrane, ν, cm^{-1}): 1779 (asym C═O, str), 1718 (sym C═O, str), 1351 (C−N, str), 819 (imide ring deformation). GPC ($CHCl_3$): M_n = 44 000 g mol^{-1}, M_w = 82 000 g mol^{-1} relative to polystyrene, M_w/M_n = 1.9. BET surface area = 760 m^2 g^{-1}, total pore volume = 0.57 cm^3 g^{-1} at (p/p_0 = 0.98, adsorption). TGA analysis: (nitrogen), thermal degradation commences at T_d ~ 405 °C.

KAUST-PI-4. Following the above general procedure, KAUST-PI-4 was prepared from the dianhydride *i*-C_3 TPDA and ODA diamine (98% yield). ^{1}H NMR (400 MHz, $CDCl_3$, δ): 1.80−1.89 (br m, 12H), 3.29−3.52 (br m, 2H), 6.91−7.8 (br m, 12H). FT-IR (membrane, ν, cm^{-1}): 1776 (asym C═O, str), 1716 (sym C═O, str), 1351 (C−N, str), 807 (imide ring deformation). GPC ($CHCl_3$): M_n = 35 000 g

mol^{-1}, M_w = 73 000 g mol^{-1} relative to polystyrene, M_w/M_n = 2.1. BET surface area = 420 m^2 g^{-1}, total pore volume = 0.282 cm^3 g^{-1} at (p/p_0 = 0.98, adsorption). TGA analysis: (nitrogen), thermal degradation commences at T_d ~ 430 °C.

KAUST-PI-5. Following the above general procedure, KAUST-PI-5 was prepared from the dianhydride *i*-C_3 TPDA and 6FpDA diamine as a pale-yellow powder (93% yield). ^{1}H NMR (400 MHz, $CDCl_3$, δ): 1.24 (br m, 6H), 1.15 (br s, 12H), 2.7 (br m, 4H), 6.94 (br s, 4H); 7.07 (br s, 2H); 7.25 (br s, 2H); 7.3 (br s, 4H); 7.37 (br s, 2H). FT-IR (KBr disk) ν = 1782 (asym C═O, str), 1728 (sym C═O, str), 1354 (C−N, str), 744 (imide ring deformation) cm^{-1}. GPC ($CHCl_3$): M_n = 42 000 g mol^{-1}, M_w = 83 000 g mol^{-1} relative to polystyrene, M_w/M_n = 2.0. BET surface area = 650 m^2 g^{-1}, total pore volume = 0.53 cm^3 g^{-1} at (p/p_0 = 0.98, adsorption). TGA analysis: (nitrogen), thermal degradation commences at T_d ~ 420 °C.

KAUST-PI-5′. Following the above general procedure, KAUST-PI-5′ was prepared from the dianhydride *n*-C_3 TPDA and 6FpdA diamine as a pale-yellow powder (84% yield). ^{1}H NMR (400 MHz, $CDCl_3$, δ): 1.41 (t, 6H), 2.15 (br m, 4H), 2.75 (br m, 4H), 6.92 (br s, 4H); 7.07 (br m, 2H); 7.29 (br s, 4H); 7.35 (br m, 2H); 7.46 (br m, 4H) 7.53 (br m, 4H). ^{19}F NMR (376 MHz, $CDCl_3$) δ (ppm): (−63.54). FT-IR (KBr disk) ν = 1778 (asym C═O, str), 1718 (sym C═O, str), 1356 (C−N, str), 746 (imide ring deformation) cm^{-1}. GPC ($CHCl_3$): M_n = 26 000 g mol^{-1}, M_w = 39 000 g mol^{-1} relative to polystyrene, M_w/M_n = 1.5. BET surface area = 430 m^2 g^{-1}, total pore volume = 0.34 cm^3 g^{-1} at (p/p_0 = 0.98, adsorption). TGA analysis: (nitrogen), thermal degradation commences at T_d ~ 405 °C.

KAUST-PI-5″. Following the above general procedure, KAUST-PI-5″ was prepared from the dianhydride C_2 TPDA and 6FpdA diamine as an off-white powder (95% yield). ^{1}H NMR (400 MHz, $CDCl_3$, δ): 1.68 (t, 6H), 2.88 (br m, 4H), 6.94 (br s, 4H); 7.07 (br m, 2H); 7.30 (br s, 4H); 7.37 (br s, 4H); 7.49 (br m, 2H) 7.52 (br m, 4H). FT-IR (KBr disk) ν = 1780 (asym C═O, str), 1724 (sym C═O, str), 1356 (C−N, str), 744 (imide ring deformation) cm^{-1}. GPC ($CHCl_3$): M_n = 15 000 g mol^{-1}, M_w = 61 000 g mol^{-1} relative to polystyrene, M_w/M_n = 4.1. BET surface area = 430 m^2 g^{-1}, total pore volume = 0.33 cm^3 g^{-1} at (p/p_0 = 0.98, adsorption). TGA analysis: (nitrogen), thermal degradation commences at T_d ~ 410 °C.

KAUST-PI-6. Following the above general procedure, KAUST-PI-6 was prepared from the dianhydride *i*-C_3 TPDA and ATAF diamine. ^{1}H NMR (400 MHz, $CDCl_3$, δ): 1.80−1.89 (br m, 12H), 2.19 (br s, 6H), 3.31−3.5 (br m, 2H), 6.91−7.8 (br m, 12H). FT-IR (membrane, ν, cm^{-1}): 1781 (asym C═O, str), 1722 (sym C═O, str), 1352 (C−N, str), 833 (imide ring deformation). GPC ($CHCl_3$): M_n = 82 000 g mol^{-1}, M_w = 135 000 g mol^{-1} relative to polystyrene, M_w/M_n = 1.6. BET surface area = 500 m^2 g^{-1}, total pore volume = 0.61 cm^3 g^{-1} at (p/p_0 = 0.98, adsorption). TGA analysis: (nitrogen), thermal degradation commences at T_d ~ 410 °C.

KAUST-PI-7. Following the above general procedure, KAUST-PI-7 was prepared from the dianhydride *i*-C_3 TPDA and DMN diamine as a pale-yellow powder (92% yield). ^{1}H NMR (400 MHz, $CDCl_3$, δ): 1.91−1.99 (br m, 12H), 2.45 (br s, 6H), 3.4−3.6 (br m, 2H), 7.06−7.65 (br m, 22H). FT-IR (membrane, ν, cm^{-1}): 1779 (asym C═O, str), 1716 (sym C═O, str), 1351 (C−N, str), 833 (imide ring deformation). GPC ($CHCl_3$): M_n = 84 000 g mol^{-1}, M_w = 140 000 g mol^{-1} relative to polystyrene, M_w/M_n = 1.7. BET surface area = 840 m^2 g^{-1}, total pore volume = 0.59 cm^3 g^{-1} at (p/p_0 = 0.98, adsorption). TGA analysis: (nitrogen), thermal degradation commences at T_d ~ 430 °C.

Dihedral Angle Modeling. Repeat units reported with bridged bicyclic and spiro contortion centers were constructed in Materials Studio 6.0 (Accelrys), and relevant dihedral angles were selected. Using the Conformer module, the dihedral angles were varied incrementally from −180° to +180°. Energy minimizations of all conformers were performed in the Forcite module using the COMPASS force field and the Smart algorithm for iterations. The energy barriers to changes in the dihedral angles were calculated relative to the lowest energy attained ($\Delta E = E_i - E_{min}$) over the 360° range. The degrees of torsional freedom available are reported at the transport testing temperature (35 °C), where the available thermal energy was approximated by 3*RT*.

Membrane Fabrication. Filtered 3−5 wt % polymer solutions in chloroform were cast on a leveled glass plate and covered to allow slow evaporation of the solvent over 2−3 days. The resulting isotropic membranes were first dried at 120 °C for 12 h in a vacuum oven, then soaked in methanol for 24 h, air-dried, and postdried at 120 °C for 24 h under high vacuum to remove any traces of residual casting solvent. Solvent removal was confirmed by TGA. Coupons were punched for gas permeation testing, with effective area and thickness determined by calibrated scanning software and a digital micrometer, respectively.

Gas Permeation Measurements. The pure-gas permeabilities of the membranes were determined using the constant-volume/variable-pressure method.[30] The membranes were degassed in the permeation test apparatus on both sides under high vacuum at 35 °C. The permeability coefficients of O_2 and N_2 were regularly measured until they varied little with time (~10−15 days). All pure-gas permeabilities were then determined. This procedure was used to allow relaxation of the nonequilibrium excess free volume contributed by methanol treatment of the membranes. The increase in permeate pressure with time was measured by an MKS Baratron transducer. The permeabilities of all gases were measured at 35 °C and 2 bar and calculated by

$$P = DS = 10^{10}\frac{V_d l}{p_{up} A R T}\frac{dp}{dt}$$

where P is the gas permeability (barrer) (1 barrer = 10^{-10} cm^3 (STP) cm cm^{-2} s^{-1} cmHg^{-1}), p_{up} is the upstream pressure (cmHg), dp/dt is the steady-state permeate side pressure increase (cmHg s^{-1}), V_d is the calibrated permeate volume (cm^3), l is the membrane thickness (cm), A is the effective membrane area (cm^2), T is the operating temperature (K), and R is the gas constant (0.278 cm^3 cmHg cm^{-3} (STP) K^{-1}). The apparent gas diffusion coefficients, D (cm^2 s^{-1}), were calculated from $D = l^2/6\theta$ where θ (s) is the time lag of gas permeation. Steady-state conditions were taken after 7−10 time lags. The solubility coefficient, S (cm^3 (STP) cm^{-3} cmHg^{-1}), was then derived from solution-diffusion theory via $S = P/D$. The ideal permselectivity ($\alpha_{A/B}$), diffusivity selectivity (α_D), and solubility selectivity (α_s) for separation of A/B was calculated by

$$\alpha_B^A = \frac{P_A}{P_B} = \frac{D_A}{D_B}\frac{S_A}{S_B} = \alpha_D \alpha_S$$

RESULTS AND DISCUSSION

Polymer Synthesis. The chemistry previously reported for the synthesis of a ladder-type spirobisindane-bearing dianhydride[12] (apparent in Figure 1) was recently modified by our

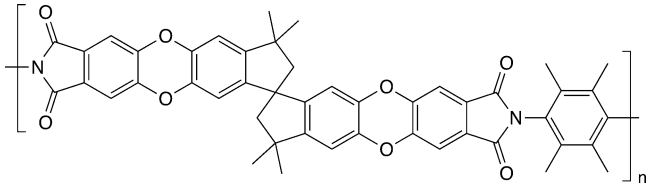

Figure 1. Structure of PIM-PI-1 based on analogous spirobisindane-based dianhydride.

group to replace the spiro centers with 9,10-diisopropyl-substituted triptycene moieties.[22] While only the isopropyl bridgehead substituent was discussed previously, the synthetic approach is versatile and can be used to integrate ethyl and propyl substituents for further investigation of the effect of the bridgehead on the microstructure and gas transport properties. It is also unique relative to other syntheses of triptycene-bearing polyimides[31−33] in that it permits infusion of the

dx.doi.org/10.1021/ma5009226 | Macromolecules 2014, 47, 5104−5114

triptycene into a fully fused-ring dianhydride, which allows the geometry of the triptycene to influence the macromolecular dynamics (e.g., intramolecular rigidity, chain propagation in space). This is apparently critical to the development of microporous polymer frameworks that are amorphous and thus retain good mechanical properties key to the membrane formation.[19,26]

Generally, the multistep synthesis begins with the preparation of the 2,3,6,7-tetramethoxy-9,10-dialkylanthracene, which then undergoes Diels–Alder addition with an in-situ-formed benzyne to form the corresponding 9,10-dialkyltriptycene in relatively high yields. Demethylation of the methoxy groups, aromatic nucleophilic substitution with 4,5-dichlorophthalonitrile, and alkaline hydrolysis yields the tetracarboxylic acid in high yield. The corresponding dianhydride is reacted with commercial diamines via a one-step, high-temperature method in *m*-cresol with catalytic amounts of isoquinoline to yield the KAUST-PI polymers in Scheme 1. All the polymers in this work were of high molecular weight (Table 1) and readily soluble in chloroform.

Table 1. Molecular Weights, Thermal Stability, and BET Surface Areas of Triptycene-Based (R = *i*-C_3, *n*-C_3, C_2) PIM-PIs

polymer	M_w (10^3 g mol^{-1})	M_w/M_n	T_d[a] (°C)	S_{BET} (m^2 g^{-1})
KAUST-PI-1	158	2.0	400	750
KAUST-PI-1′	72	1.5	415	610
KAUST-PI-2	120	1.8	402	740
KAUST-PI-3	82	1.9	405	760
KAUST-PI-4	73	2.1	430	420
KAUST-PI-5	83	2.0	420	650
KAUST-PI-5′	39	1.5	405	430
KAUST-PI-5″	61	4.1	410	430
KAUST-PI-6	135	1.6	410	500
KAUST-PI-7	140	1.7	430	840

[a]Approximate temperature at onset of decomposition.

Physical Properties of PIM-PIs. As expected for polyimides, the KAUST-PI materials demonstrated high thermal stability, with decomposition temperatures exceeding 400 °C (Table 1). No glass transition temperatures were observed before the decomposition temperature (T_d) as reported for spiro-based[12] and triptycene-based[31] polyimides, indicating the high intramolecular rigidity characteristic of PIM-type materials. KAUST-PI-7, prepared by reaction of DMN with the *i*-C_3 TPDA (Scheme 1) dianhydride, displayed the highest BET surface area (840 m^2 g^{-1}) reported to date for polyimides as measured by nitrogen adsorption at 77 K (Table 1). Upon replacing the spiro center of structurally analogous PIM-PIs[12] (Figure 1) with the 9,10-diisopropyltriptycene moiety, surface areas generally increased regardless of the diamine—e.g., DMN (680–840 m^2 g^{-1}), TMPD (680–750 m^2 g^{-1}), and 6FpDA (470–650 m^2 g^{-1}). For the ATAF-based polyimides, the change in surface area was negligible. Furthermore, with bulky and rigid diamines that are substituted to restrict rotation at the imide bond (e.g., TMPD, TrMPD, and DMN) the gas uptake and surface areas approached those of ladder-type PIMs including PIM-1 (770 m^2 g^{-1}) and extremely permeable substituted polyacetylenes like poly[1-(trimethylsilyl)-1-propyne] (PTMSP) (950 m^2 g^{-1}) (Figure S1, Supporting Information). Together with previous work on ethanoanthracene and Tröger's base moieties,[8] this suggests that the infusion of three-dimensional and shape-persistent bridged bicyclics into fully fused-ring backbones is more favorable for disrupting chain packing and developing amorphous, microporous polymeric structures. Similarly, Long and Swager provided the earliest report of rotation-restricting multiple-point attachments of bulky triptycene moieties to polymer backbones as an efficient means to low-*K* dielectric materials.[6] When triptycene is instead incorporated into polyimides as a freely rotating diamine, the surface areas—and hence microporosity—decrease considerably and range from 39 to 121 m^2 g^{-1}.[31,32]

Interestingly, large reductions in BET surface area were observed when a linear alkyl chain was used at the bridgehead in place of the branched isopropyl chain. For example, the surface area for the 6FpDA-based KAUST-PI-5 (R = *i*-C_3) and KAUST-PI-5′ (R = *n*-C_3) dropped ~30% from 650 m^2 g^{-1} (*i*-C_3) to 430 m^2 g^{-1} (*n*-C_3). Similarly for the TMPD-based KAUST-PI-1 (R = *i*-C_3) and KAUST-PI-1′ (R = *n*-C_3), a ~20% drop from 750 m^2 g^{-1} (*i*-C_3) to 610 m^2 g^{-1} (*n*-C_3) was measured (Table 1). Furthermore, Figure 2 qualitatively

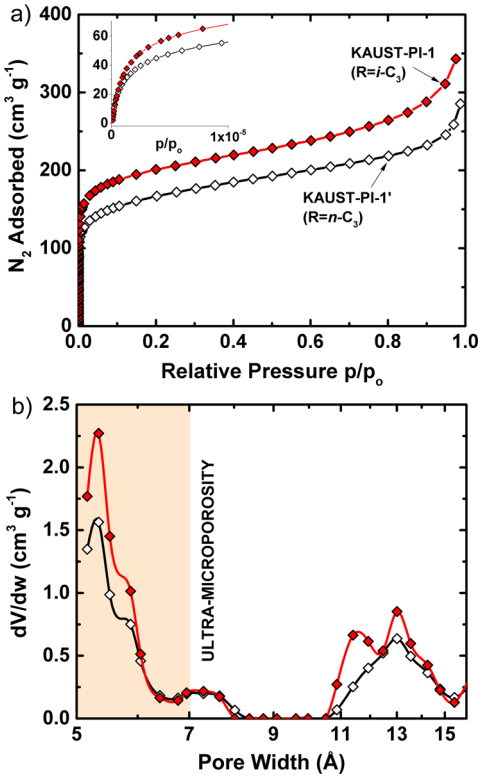

Figure 2. (a) Nitrogen adsorption isotherms (T = 77 K, p_0 = 1 bar) and (b) NLDFT-derived pore-size distributions for KAUST-PI-1 and KAUST-PI-1′ elucidating the effect of 9,10-bridgehead-substitution on the microstructures. Inset in (a) zoomed to $p/p_0 = 1 \times 10^{-5}$.

elucidates the differences in the microstructures resulting from linear (KAUST-PI-1′) and branched (KAUST-PI-1) bridgehead substituents.[34] The inset of Figure 2a reveals a steeper increase in gas sorption and larger uptakes for the *i*-C_3-substituted polymer at very low pressures ($p/p_0 < 10^{-5}$) where sorption in micropores preferentially occurs. The NLDFT-derived pore-size distributions of Figure 2b show a bimodal distribution in microporosity, which is typical of PIMs, detailing a significant increase in the fraction of smaller, molecularly dimensioned pores in the *i*-C_3-substituted polymer concom-

dx.doi.org/10.1021/ma5009226 | Macromolecules 2014, 47, 5104–5114

itant with a slight increase in the fraction of larger pores. Hypothesizing that the larger pores are interconnected through the smaller pores, this auspicious introduction of finer ultramicroporosity (<7 Å) along with some larger pores induced by the short and bulky branched substituent should enhance diffusion-based gas transport.

The mechanical properties of polymers designed for gas separation are critical to their fabrication into industrially relevant thin films that are densely packed into spiral-wound or hollow-fiber modules. Table 2 summarizes the tensile behavior

Table 2. Mechanical Properties of PIMs in the Elastic Region and at Break

		at break	
polymer	Young's modulus (MPa)	elongation (%)	tensile strength (MPa)
KAUST-PI-1	2460	5.9	94
PIM-PI-1	1620	69	61
6FDA-DATRI[32]		4.5	62
PIM-EA-TB	~1000		
PIM-TRIP-TB[9]	1206	*a*	45
PIM-1[36]	868[b]	10	48
PTMSP[37]	630	73	40
Matrimid[d]	2896	49	85

[a]Large deviations were observed in elongation. [b]Young's modulus measured elsewhere.[22] [d]Available from the supplier (www.lindberg-lund.com).

in the elastic region (low strains, Young's modulus) and at break for relevant spiro- and triptycene-based polyimides as well as traditional PIMs including PIM-1 and PTMSP and more recent Tröger's base PIMs. Substitution of the spiro-center in PIM−PI-1 with the more shape-persistent 9,10-diisopropyl-triptycene in KAUST-PI-1 results in a 150% increase in Young's modulus to 2460 MPa and a 50% increase in tensile strength at break to 94 MPa. The spiro-based PIM−PI-1, on the other hand, can endure significantly higher strains (reaching 69%) probably due to unwinding of the chains from a highly entangled state spurred by the geometry of the spiro moiety (flexible 90° kink). This mechanical flexibility has been also observed for polybenzoxazoles obtained from thermal rearrangement of *o*-hydroxy polyimides containing spirobisindane.[35] Elongation is slightly compromised in PIM-1 probably due to its ladder-type backbone. Despite the reductions in maximum elongation of KAUST-PI-1, films (70−100 μm) are easily handled and can be "creased" without breaking.[22] Interestingly, slightly higher elongations and significantly greater tensile strengths are observed for KAUST-PI-1 relative to 6FDA-DATRI,[32] indicating that the integration of triptycene into the rigid fused-ring dianhydride instead of as a loosely connected diamine also leads to more mechanically robust polymers. Particularly, the mechanical strengths and elasticities of PIM-PIs and PIMs designed with triptycene-based contortion centers approach those of Matrimid, which is employed industrially in membrane-based gas separations.

Geometric Modeling. The differences in macroscopic mechanical properties of the polymer membranes are closely related to the molecular structures of their constituent backbones. The degrees of torsional freedom—i.e., span of accessible angles—at the transport testing temperature (35 °C) for select dihedral angles in different contortion sites are presented in Figure 3. The bridged bicyclics including triptycene (TRIP), ethanoanthracene (EA), and Tröger's base (TB) have up to ~50% less torsional freedom than the spiro center used in the previous PIM-PIs and early ladder PIMs PIM-1 and PIM-7. The EA is slightly more torsion-resistant than TB, as also reported from equilibrated packing simulations[38] but only slightly more flexible than the triptycene moiety which has an additional vertical aromatic ring. The increased rigidity of bridged bicyclic contortion sites support the improved mechanical strength and Young's modulus observed for triptycene-based KAUST-PI-1 relative to its spiro-based analogue, PIM-PI-1 (Table 2). They also support the increases in accessible surface areas corresponding to enhanced development of microporosity (Table 1). That is, the development of microporosity depends largely on the ability of a contortion center to resist molecular deformation and maintain the intramolecular rigidity that disrupts chain packing.[19,26]

Gas Transport Properties: 9,10-Diisopropyl-Triptycene-Based KAUST-PIs. The pure-gas transport properties of all polyimides derived from 9,10-diisopropyl-substituted triptycene are reported at 2 bar and 35 °C in Tables 3 and 4. For all polymers except KAUST-PI-7, the order of the permeabilities follows $H_2 > CO_2 > He > O_2 > N_2 \sim CH_4$. This order is opposite to that observed for prototypical PIM-1 and PTMSP[39] where solubility contributes strongly to gas transport and appreciably higher permeabilities are measured for CO_2 than H_2 and likewise for CH_4 than N_2. As a result, both PIM-1 and PTMSP demonstrate unique solubility-driven

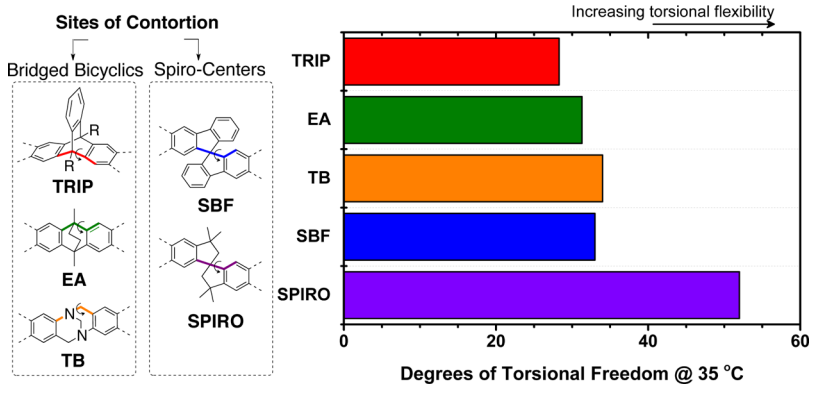

Figure 3. Molecular simulation of dihedral angle distributions for bridged-bicyclic and spiro-based sites of contortion. The range of accessible angles is reported for each assuming an available thermal energy of 3*RT*.

dx.doi.org/10.1021/ma5009226 | *Macromolecules* 2014, 47, 5104−5114

Table 3. Gas Permeabilities and Permselectivities for 9,10-Diisopropyltriptycene-Based KAUST-PI Membranes at 35 °C and 2 bar

	permeability[a] (barrers)						permselectivity				
polymer	He	H_2	N_2	O_2	CH_4	CO_2	O_2/N_2	H_2/N_2	H_2/CH_4	CO_2/N_2	CO_2/CH_4
KAUST-PI-1	1771	3983	107	627	105	2389	5.9	37	38	33	23
KAUST-PI-2	1026	2368	98	490	101	2071	5.0	24	23	21	21
KAUST-PI-3	862	1625	43	238	43	916	5.5	38	38	21	21
KAUST-PI-4	176	302	10.6	48	10.7	286	4.5	29	28	27	27
KAUST-PI-5	816	1558	87	356	77	1552	4.1	18	20	18	20
KAUST-PI-6	278	409	14.4	64.8	11	322	4.5	28	37	22	29
KAUST-PI-7	1371	3198	225	842	354	4391	3.7	14	9	20	12
Matrimid[1]		18	0.32	2.1	0.28	10	6.6	56	64	31	36

[a] 1 barrer = 10^{-10} cm^3 (STP) cm cm^{-2} s^{-1} $cmHg^{-1}$.

Table 4. Gas Diffusivities, Solubilities, and Selectivities for 9,10-Diisopropyltriptycene-Based KAUST-PI Membranes at 35 °C and 2 bar

	D (10^{-8} cm^2 s^{-1})				S (10^{-2} cm^3 cm^{-3} $cmHg^{-1}$)				O_2/N_2		CO_2/CH_4	
polymer	N_2	O_2	CH_4	CO_2	N_2	O_2	CH_4	CO_2	α_D	α_S	α_D	α_S
KAUST-PI-1	31.2	158	9.51	45.6	3.43	3.98	11.2	53.3	5.06	1.16	4.79	4.76
KAUST-PI-2	28.9	138	8.00	49.3	3.39	3.56	12.6	42.0	4.78	1.05	6.16	3.33
KAUST-PI-3	14.6	70.7	4.20	22.5	2.97	3.36	10.2	40.6	4.84	1.13	5.36	3.98
KAUST-PI-4	3.18	13.1	0.871	6.81	3.35	3.62	12.3	42.1	4.12	1.08	7.82	3.42
KAUST-PI-5	22.7	86.2	5.82	34.7	3.83	4.13	13.3	44.8	3.80	1.08	5.96	3.37
KAUST-PI-6	6.43	25.8	1.38	10.9	2.23	2.51	7.98	29.7	4.01	1.13	7.90	3.72
KAUST-PI-7	48.9	177	19.1	85.3	4.60	4.75	18.5	47.9	3.62	1.03	4.47	2.59

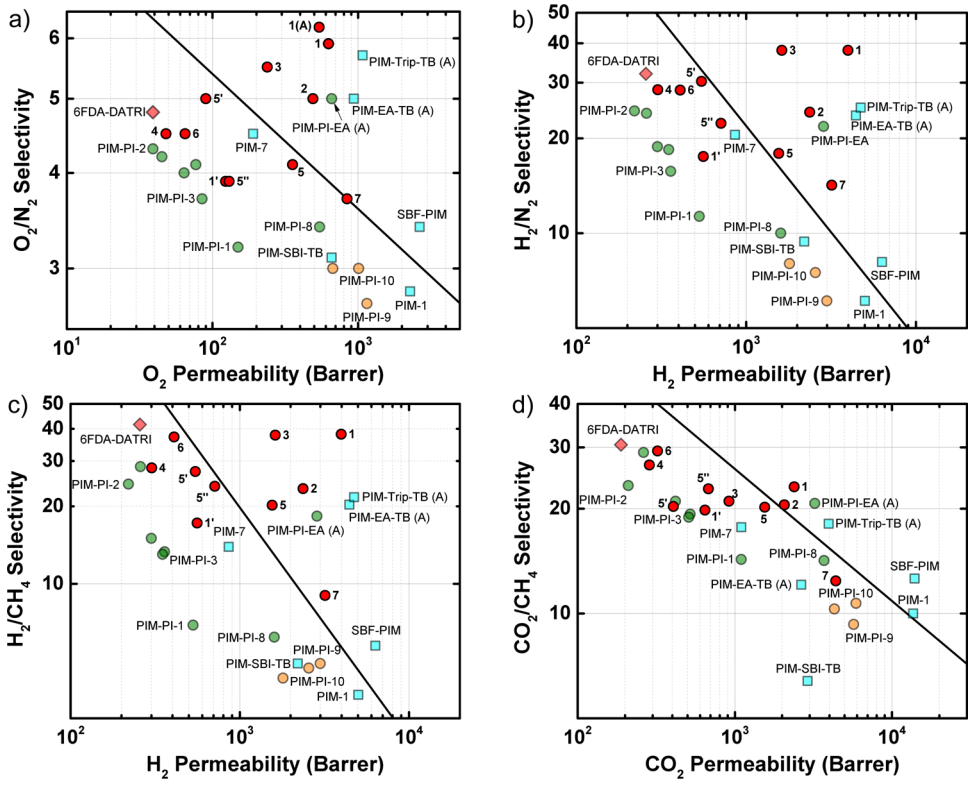

Figure 4. Gas separation performance of KAUST-PIs containing 9,10-bridgehead-substituted triptycene for (a) oxygen enrichment, hydrogen recovery from (b) ammonia purge gases, and (c) petrochemical refinery streams as well as (d) natural gas sweetening. Polymers are enumerated as indicated in Scheme 1. "1A" refers to KAUST-PI-1 O_2/N_2 performance after 150 days. The solid lines represent 2008 permeability/selectivity trade-offs.[29]

"reverse-selective" transport with preferential permeation of large hydrocarbons over smaller gases.[40−43] On the contrary, and as supported by comparative nitrogen sorption experiments on PIM-1, PTMSP, and KAUST-PI-1 (Figure S1, Supporting Information), locking the 9,10-diisopropyltriptycene moiety in a fused ring dianhydride results in a pore-size distribution

dx.doi.org/10.1021/ma5009226 | Macromolecules 2014, 47, 5104−5114

Table 5. Effect of the Dianhydride (Site of Contortion) and Diamine on the Development of Gas Transport Properties Upon Transitioning from Low-Free-Volume Polyimides to High-Free-Volume PIM-Polyimides

polyimide		permeability (barrers)					permselectivity			O_2/N_2		CO_2/CH_4	
diamine	dianhydride	H_2	N_2	O_2	CH_4	CO_2	H_2/CH_4	O_2/N_2	CO_2/CH_4	α_D	α_S	α_D	α_S
TMPD	*i*-C_3 TPDA	3983	107	627	105	2389	37.9	5.9	22.8	5.06	1.16	4.79	4.76
	Spiro *(Ext)*[a]	530	47	150	77	1100	6.9	3.2	14.3	2.80	1.17	2.43	5.64
	Spiro *(Non-Ext)*[b]	2990	420	1150	610	5700	4.9	2.7	9.3	2.68	1.03	2.68	3.51
	6FDA[c]	549	35.6	122	28.2	440	19.5	3.4	15.6	2.87	1.27	5.00	3.17
6FpDA	*i*-C_3 TPDA	1558	87	356	77	1552	20.2	4.1	20.2	3.80	1.08	5.96	3.37
	Spiro *(Ext)*[a]	360	23	85	27	520	13.3	3.7	19.3	3.20	1.13	4.00	4.73
	6FDA[d]	108	3.11	14.2	1.34	51.2	80.6	4.6	38.2	3.57	1.41	12.3	3.15
DMN	*i*-C_3 TPDA	3198	225	842	354	4391	9.0	3.7	12.4	3.62	1.03	4.47	2.59
	EA[e,24]	4230	369	1380	457	7340	9.3	3.7	16	3.21	1.16	3.96	4.07
	Spiro *(Ext)*[a]	1600	160	545	260	3700	6.2	3.4	14.2	3.17	1.05	3.21	4.50
	Spiro *(Non-Ext)*[e]	2560	340	1010	550	5910	4.7	3.0	10.7	2.78	1.05	3.30	2.95
	6FDA[44]	812	61.4	213	71.8	1357	11.3	3.5	18.9	2.64	1.31	4.29	4.41
p,p′-ODA	*i*-C_3 TPDA	302	10.6	48	10.7	286	28.2	4.5	26.7	4.12	1.08	7.82	3.42
	6FDA[d]	40.7	0.73	3.88	0.34	16.7	120	5.3	49	4.00	1.33	14.1	3.38
TrMPD	*i*-C_3 TPDA	4563	161	814	161	3140	28.4	5.1	19.5	4.36	1.16	6.00	3.26
	6FDA[c]	516	31.6	109	26	431	19.8	3.5	16.6	2.68	1.23	5.45	3.08

[a]Testing conditions: 30 °C, 200−300 mbar.[13] [b]25 °C, 1 bar.[23] [c]35 °C, 10 bar.[47] [d]35 °C, 2 bar.[48] [e]25 °C, 1 bar.[24]

comprising both smaller *and* larger porosities, where the presence of the smaller pores elicits enhancements in molecular sieving. The resulting polymers demonstrate combinations of permeabilities and selectivities significantly surpassing state-of-the-art polymers for key gas separations (Figure 4). Outstanding air (O_2/N_2) (Figure 4a) and hydrogen (H_2/N_2, H_2/CH_4) (Figure 4b,c) separation performance is observed particularly for the KAUST-PIs derived from rotation-restricted TMPD (1), TMBZ (2), and TrMPD (3) diamines. Polymers derived from ODA (4) and ATAF (6) maintain reasonably high selectivities but show appreciable losses in permeability. This may be due to an improved chain packing incurred by their inherent flexibilities. In addition, both the TrMPD (3) and ODA (4) polymers have higher selectivities, and in the case of the ODA, far higher permeabilities than predicted for their spiro-based counterparts.[12] The anomalous behavior by KAUST-PI-7, which displayed the highest BET surface area (840 $m^2\ g^{-1}$), highest gas permeabilities—except for He and H_2—and lowest gas selectivities of the series, may be attributed to an excessive "opening" of the microstructure due to the very bulky architecture of the DMN diamine. This compromises diffusivity selectivity to reduce overall permselectivity. Interestingly, the same behavior has also been reported for DMN-based polyimides derived from 6FDA[44] and the recent PIM-type spiro- and ethanoanthracene-based dianhydrides[24] (Table 5). Compared to commercial Matrimid membranes ($P(O_2)$ = 2.1 barrer, $\alpha(O_2/N_2)$ = 6.6),[1] KAUST-PIs of sufficient intramolecular rigidity can exhibit up to 300-fold higher O_2 permeabilities with only 10% lower O_2/N_2 selectivities. Based on Figure 4, they possess some of the most promising combinations of permeabilities and selectivities among reported PIMs for air and hydrogen separations accounting for more than 75% of the membrane-based gas separation market.

Considering the avid research targeting more permeable and selective polyimide gas separation membranes, Table 5 summarizes gas transport properties for polyimides containing various contortion-center-bearing dianhydrides and different aromatic diamines to identify insightful structure/property relationships that can serve as design guides. The dianhydrides include the (i) established 6FDA[45,46] common to some of the best performing low-free-volume polyimides, (ii) extended spirobisindane-based dianhydride (Spiro (*Ext*))[12] serving as the platform for the earliest PIM-PIs, (iii) its nonextended analogue (Spiro (*Non-Ext*)),[23] and (iv) emerging bridged-bicyclic-based dianhydrides employing ethanoanthracene (EA)[24] and 9,10-diisopropyl-substituted triptycene (*i*-C_3 TPDA).[22]

Table 5 demonstrates that for diamines highly substituted to restrict rotation about the imide bond (e.g., TMPD, TrMPD, and DMN) and thus increase intrachain rigidity, permeability gains are concurrent with selectivity losses upon transitioning from low-free-volume 6FDA-based polyimides to high-free-volume spirobisindane-based PIM-PIs (extended and nonextended). However, selectivity can be recovered and *significantly increased* (TrMPD, TMPD) when the 9,10-diisopropyltriptycene-based dianhydride is used. For example, going from 6FDA → Spiro(*Ext*) → Spiro(*Non-Ext*) → *i*-C_3 TPDA with TMPD as a diamine, the O_2 permeability proceeds from 122 → 150 → 1150 → 627 barrers while the O_2/N_2 selectivity proceeds from 3.4 → 3.2 → 2.7 → 5.9. Ultimately, a ∼5-fold increase in permeability concomitant with a 70% increase in selectivity is observed by replacing 6FDA with *i*-C_3 TPDA. A similar trend is observed with the DMN diamine, where the EA dianhydride yields improved selectivities and permeabilities over the spiro dianhydrides, further promoting the use of rigid and fused-ring bridged bicyclics over flexible spiro contortion centers. There, however, the selectivities of the low-free-volume polyimides are not matched in the PIM-PIs. The increase in free volume gained by a severe disruption of chain packing caused by the bulky structure of DMN outweighs the intrachain rigidity gained. The enhancements in the selectivity and permeability for gas transport through PIM-PIs based on bridged bicyclics upon use of methyl-substituted diamines is opposite to what was previously observed for 6FDA-polyimides, where large reductions in permselectivities were concurrent with large increases in permeability upon methyl substitution of the diamines.[47] The PIM-PIs demonstrate improved performance for the O_2/N_2 gas pair as a result of improved diffusivity *and* diffusivity selectivities. Noted are the different considerations that must be made in designing

dx.doi.org/10.1021/ma5009226 | *Macromolecules* 2014, 47, 5104−5114

Table 6. Effect of Bridgehead Substituent on BET Surface Areas and Gas Permeabilities of Triptycene-Based KAUST-PIs

					permeability (barrers)				
polymer	diamine	R	S_{BET} (m^2 g^{-1})	He	H_2	N_2	O_2	CH_4	CO_2
KAUST-PI-5″	6FpDA	C_2	430	454	712	32	126	30	679
KAUST-PI-5′		*n*-C_3	430	292	546	18	90	20	406
KAUST-PI-5		*i*-C_3	650	816	1558	87	356	77	1552
KAUST-PI-1′	TMPD	*n*-C_3	610	314	560	32	123	33	645
KAUST-PI-1		*i*-C_3	750	1771	3983	107	627	105	2389

PIM-PI structures with pore-size distributions tailored for molecular sieving.[45]

Furthermore, by replacing the 6FpdA diamine with the TMPD diamine, gas transport properties respond differently depending on the contortion center and the gas pair. The O_2 permeabilities improve (75%) for the structurally analogous Spiro (*Ext*) and *i*-C_3 TPDA dianhydrides, but O_2/N_2 selectivity improves 45% (4.1 to 5.9) for the *i*-C_3 TPDA while it drops 14% (3.7 to 3.2) for the Spiro (*Ext*). Similarly, for the H_2/CH_4 gas pair, *i*-C_3 TPDA elicits a more exaggerated 90% increase in selectivity (20 to 38) along with a 250% increase in H_2 permeability (1558 to 3983 barrers), while the Spiro (*Ext*) moiety causes a 150% increase in H_2 permeability (360 to 530 barrers) but a severe 50% (13.3 to 6.9) drop in selectivity. The behavior for the CO_2/CH_4 gas pair is qualitatively similar, but the improvement in performance for the *i*-C_3 TPDA is primarily permeability-based. That is, Figure 4d illustrates that although the bridged-bicyclic-based PIM-PIs (*i*-C_3 TPDA and EA) surpass the spiro-based PIM-PIs, the strides in performance apparent for the O_2 and H_2 gas pairs are not as evident for the CO_2/CH_4 gas pair, where a trade-off relationship is generally obeyed. Unlike for the O_2 and H_2 gas pairs, Tables 3 and 4 demonstrate that the least permeable and, hence, most densely packed ODA- (KAUST-PI-4) and ATAF-based (KAUST-PI-6) polyimides exhibit the highest CO_2/CH_4 permselectivities owing to the highest diffusivity selectivities (e.g., 60% higher $\alpha_D(CO_2/CH_4)$ than KAUST-PI-1). In addition, other PIM-PIs in the literature that do not integrate contortion centers in a rigid fashion and are more densely packed (e.g., spiro-based PIM-6FDA-OH[21] and triptycene-based 6FDA-DATRI[31,32]) also show more selective (diffusivity-based) CO_2/CH_4 separation. Generally, pure-gas results for gas pairs involving condensable gases can mask nonideal effects like plasticization and competitive sorption, and thus the mixed-gas CO_2/CH_4 transport properties of these polyimides are currently under investigation.

Interestingly, the nonextended spirobisindane-based structures exhibit up to 10-fold higher gas permeabilities but almost consistently 50% lower gas selectivities than analogous extended-spirobisindane structures for key gas pairs including H_2/CH_4, O_2/N_2, and CO_2/CH_4 (Table 5). The nonextended form contains a higher concentration of the spirobisindane moiety per unit volume. On the contrary, analogous nonextended structures based on the bridged bicyclic ethanoanthracene (e.g., EA-DMN) demonstrate much higher permeabilities *and* 50% higher selectivities near those reported for triptycene-based polyimides. Given the similarity of the backbones, these transport properties indicate that the geometries of the bridged bicyclics and the manner in which they influence chain growth is important. That is, both ethanoanthracene and triptycene constrain the growth of the macromolecule in a planar and ribbon-like fashion.[22] Spiro-centers, on the other hand, spur an erratic growth that leads to a more highly coiled macromolecule that sacrifices some of the finer microporosity responsible for sieving.

A similar analysis concluded in 1988 that any change to the structure of a polyimide should strike a balance between gains and losses in both the *inter*segmental spacing and the *intra*segmental mobility.[46] That is, a change that disrupts packing while simultaneously increasing the resistance to motion about mobile joints in the chains was observed to improve the gas permeability while either maintaining or even boosting the gas selectivity. This remains consistent with the trends observed here for PIM−PIs.

Gas Transport Properties: Effect of Bridgehead Substituent. As indicated by the pore-size distributions derived from nitrogen sorption isotherms (Figure 2) for KAUST-PI-1 and KAUST-PI-1′, the bridgehead substituent has a notable impact on the polymer microstructure. To further investigate this, transport properties (*P*, *D*, and *S*) and BET surface areas for KAUST-PI-1 and KAUST-PI-1′ as well as KAUST-PI-5 (R = *i*-C_3), -5′ (R = *n*-C_3), and -5″ (R = C_2) were measured. Table 6 shows that for both diamines the permeabilities and surface areas are largest when the bridgehead is the branched isopropyl chain. Moreover, as observed above, the effect on gas permeability upon replacing propyl with isopropyl also depends on the diamine: (i) He and H_2 permeabilities increase 6−7-fold with TMPD, ∼3-fold with 6FpDA; (ii) N_2 permeabilities increase ∼3-fold with TMPD, ∼5-fold for 6FpdA; (iii) O_2 permeabilities increase ∼5-fold with TMPD, 4-fold with 6FpdA; (iv) CH_4 permeabilities increase 3-fold with TMPD, ∼4-fold with 6FpDA; and (v) CO_2 permeabilities respond with a ∼4-fold increase for both diamines. TMPD permits larger increases in the permeabilities of the smaller gases He (kinetic diameter k_D = 2.6 Å), H_2 (k_D = 2.9 Å), and O_2 (k_D = 3.3 Å) than the larger N_2 (k_D = 3.64 Å) and CH_4 (k_D = 3.80 Å) gases, supporting the hypothesis that the microstructure adopts more pronounced ultramicroporosity. This is further corroborated by an improved diffusivity selectivity (3.8 to 5.1) for O_2/N_2 observed for the TMPD polymers but not those containing the more freely rotating 6FpDA (Table S1, Supporting Information).

The effect of the bridgehead substituent on the solubility coefficients is consistent (Table S1, Supporting Information) with results from gas sorption in network polymers containing bridgehead-substituted triptycene.[5] Fixing 6FpdA as the diamine, using a shorter C_2-bridgehead substituent (KAUST-PI-5″) results in a general permeability increase of 50% due to large improvements in the solubility coefficients. However, while the absolute value of the solubility is improved the solubility selectivity remains constant as expected for polymers of a given class[49] (Table S1, Supporting Information). In the *n*-C_3-substituted KAUST-PI-5′, even though permeability coefficients are lower, diffusivity coefficients are higher than in the C_2-substituted KAUST-PI-5″, which may be due to an improved mobility of the more flexible, longer *n*-C_3 side

dx.doi.org/10.1021/ma5009226 | *Macromolecules* 2014, 47, 5104−5114

chains.[50] ^{13}C NMR studies have indicated the triptycene cannot efficiently restrict reorientation of the CH_3 groups that are more distant.[5] Concisely, the balance between *inter*segmental spacing and *intra*segmental mobility is optimized in this study with the combination of short, bulky isopropyl substituents and rigid torsion-resistant diamines. This was also reported for isopropyl side chains on substituted polyacetylenes.[51]

Gas Transport Properties: Significance of an "Aging Knee" in PIMs. The gas transport properties of intrinsically microporous materials are time-dependent owing to an aging phenomenon by which the structure compacts into a more tightly packed equilibrium state.[52] This behavior is pronounced post-film conditioning, in which a nonsolvent like methanol swells the polymer to facilitate the removal of casting solvent trapped in the micropores. Therefore, a simple protocol was established in this study to identify an "aging knee" at which quasi-steady-state, and hence more practical and representative, transport properties could be reported. The permeability, diffusivity, and solubility coefficients for KAUST-PI-1 were monitored over a 150 day period after methanol conditioning and are presented in Figure 5. In the first 10−15 days, rapid

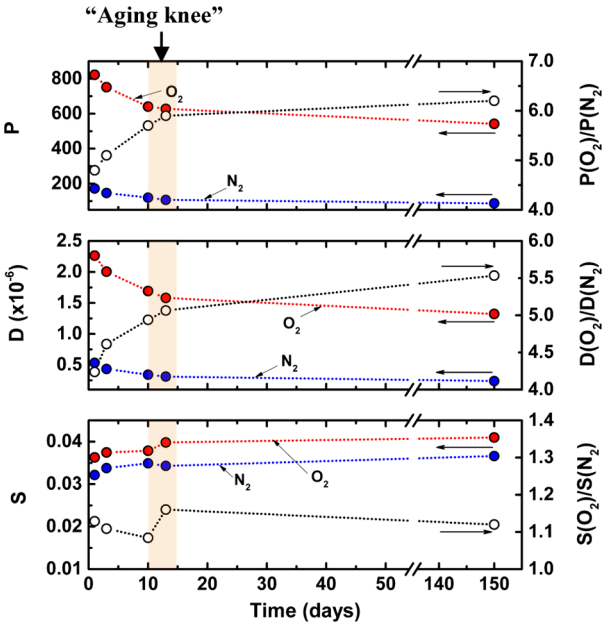

Figure 5. Identification of an "aging knee" where time dependence of gas transport properties in methanol-conditioned KAUST-PI-1 is mitigated and a quasi-steady state is reached. Units: P [barrers] (10^{-10} cm^3 (STP) cm cm^{-2} s^{-1} cmHg^{-1}); D (cm^2 s^{-1}); S (cm^3 (STP) cm^{-3} cmHg^{-1}).

drops in O_2 and N_2 permeabilities are governed by an equivalent drop in diffusivity as nonequilibrium excess free volume dissipates. This drop is more significant for the larger N_2 gas, and thus rapid rises in O_2/N_2 diffusivity selectivities and overall permselectivities are observed. After 15 days ($P(O_2)$ = 627, $\alpha(O_2/N_2)$ = 5.9), further changes are modest even up to 150 days ($P(O_2)$ = 542, $\alpha(O_2/N_2)$ = 6.2). Point "1A" measured at 150 days is plotted in Figure 4a for comparison with data for PIM-EA-TB (A), PIM-PI-EA (A), and PIM-TRIP-TB (A), which were *aged* over a range of 100−300 days. Interestingly, the general time frame of 10−15 days observed for an "aging knee" in KAUST-PI-1—and the other polymers of this study—was also reported for ladder-type PIM-1.[53] All data in this article were reported in this fashion, and the authors generally recommend that the transport properties of PIMs be so presented to permit better fundamental *and* practical evaluations of the rapidly emerging data in this growing area of research.

CONCLUSIONS

In this article, an extensive study (including the synthesis of two new triptycene-based dianhydrides and eight new polyimides) exploring the effects of various structural features (e.g., contortion center geometry, diamine bulkiness and methyl substitution, bridgehead substituent on triptycene) on the microstructural, mechanical, and gas transport properties of PIM-type polyimides elucidated valuable structure/property relationships. In conjunction with data available in the literature, specific design principles are deduced that target a balance between *inter*segmental spacing and *intra*segmental mobility and achieve ultramicroporous polymers suitable for molecular sieving. Upon progressing from low-free-volume conventional polyimides to high-free-volume PIM-PIs, the trade-offs in permeability and selectivity embodied by the upper bounds to polymeric gas separation performance may be overcome and redefined for sieving-based air and hydrogen separations if:

(i) Contortion sites are chosen as shape-persistent bridged bicyclics that are integrated *rigidly* into the backbone such that their unique geometries (kink angle, rigidity) can strongly influence growth and packing of the macromolecule. Polyimides incorporating ethanoanthracene and 9,10-diakyltriptycene (both ∼120° kink) into fully fused ring dianhydrides have demonstrated gains in permeability and selectivity over conventional low-free-volume 6FDA-based polyimides.

(ii) Short diamines are used that restrict rotation about the imide bond to restrict *intra*molecular flexibility, further exaggerating the effects of the contortion site on chain dynamics. Contrary to previous reports with 6FDA-based polyimides, the present work on triptycene-based polyimides indicates that methyl-substituted diamines (TrMPD, TMPD, TMBZ) can simultaneously boost permeability and selectivity. However, the gains in intersegmental spacing caused by DMN outweigh the gains in *intra*molecular inflexibility and significantly increase permeability at the expensve of selectivity.

(iii) The bridgehead on the 9,10-dialkyltriptycene moiety is preferably chosen as a short, bulky isopropyl chain. Permeability and selectivity are compromised when ethyl and propyl chains are used at the bridgehead.

(iv) The bridged bicyclic contortion centers (e.g., ethanoanthracene) are concentrated in the repeat unit.

Moreover, the spirobisindane moiety imparts excellent elongation properties to the polyimides that are compromised for large gains in tensile strengths with the use of more rigid bridged bicyclics. Finally, the outstanding strides in gas separation performance over low-free-volume polyimides for air and hydrogen separations are not achieved for the increasingly important CO_2/CH_4 separation. Identification of the relevant structural features is currently being pursued.

ASSOCIATED CONTENT

Supporting Information

Detailed synthesis and characterizations of all monomers leading to dianhydrides, nitrogen adsorption isotherms and NLDFT-based pore-size distributions for PIM-1 and PTMSP, diffusivity and solubility coefficients for 9,10-diethyl- and 9,10-

dx.doi.org/10.1021/ma5009226 | Macromolecules 2014, 47, 5104−5114

dipropyltriptycene-containing polyimides. This material is available free of charge via the Internet at http://pubs.acs.org.

AUTHOR INFORMATION

Corresponding Author

*E-mail: Ingo.Pinnau@kaust.edu.sa (I.P.).

Notes

The authors declare no competing financial interest.

ACKNOWLEDGMENTS

This work was supported by KAUST funding for Prof. Ingo Pinnau. The authors thank Prof. N. B. McKeown (University of Edinburgh) and Dr. Caterina Grazia Bezzu for gel permeation chromatography measurements.

REFERENCES

(1) Sanders, D. E.; Smith, Z. P.; Guo, R. L.; Robeson, L. M.; McGrath, J. E.; Paul, D. R.; Freeman, B. D. *Polymer* **2013**, *54*, 4729−4761.

(2) Du, N. Y.; Park, H. B.; Dal-Cin, M. M.; Guiver, M. D. *Energy Environ. Sci.* **2012**, *5*, 7306−7322.

(3) McKeown, N. B.; Ghanem, B.; Msayib, K. J.; Budd, P. M.; Tattershall, C. E.; Mahmood, K.; Tan, S.; Book, D.; Langmi, H. W.; Walton, A. *Angew. Chem., Int. Ed.* **2006**, *45*, 1804−1807.

(4) Yaghi, O. M.; O'Keeffe, M.; Ockwig, N. W.; Chae, H. K.; Eddaoudi, M.; Kim, J. *Nature* **2003**, *423*, 705−714.

(5) Ghanem, B. S.; Hashem, M.; Harris, K. D. M.; Msayib, K. J.; Xu, M. C.; Budd, P. M.; Chaukura, N.; Book, D.; Tedds, S.; Walton, A.; McKeown, N. B. *Macromolecules* **2010**, *43*, 5287−5294.

(6) Long, T. M.; Swager, T. M. *J. Am. Chem. Soc.* **2003**, *125*, 14113−14119.

(7) Budd, P. M.; Msayib, K. J.; Tattershall, C. E.; Ghanem, B. S.; Reynolds, K. J.; McKeown, N. B.; Fritsch, D. *J. Membr. Sci.* **2005**, *251*, 263−269.

(8) Carta, M.; Malpass-Evans, R.; Croad, M.; Rogan, Y.; Jansen, J. C.; Bernardo, P.; Bazzarelli, F.; McKeown, N. B. *Science* **2013**, *339*, 303−307.

(9) Carta, M.; Croad, M.; Malpass-Evans, R.; Jansen, J. C.; Bernardo, P.; Clarizia, G.; Friess, K.; Lanč, M.; McKeown, N. B. *Adv. Mater.* **2014**, DOI: 10.1002/adma.201305783.

(10) Bezzu, C. G.; Carta, M.; Tonkins, A.; Jansen, J. C.; Bernardo, P.; Bazzarelli, F.; McKeown, N. B. *Adv. Mater.* **2012**, *24*, 5930−5933.

(11) McKeown, N. B. *ISRN Mater. Sci.* **2012**, *2012*, 16.

(12) Ghanem, B. S.; McKeown, N. B.; Budd, P. M.; Al-Harbi, N. M.; Fritsch, D.; Heinrich, K.; Starannikova, L.; Tokarev, A.; Yampolskii, Y. *Macromolecules* **2009**, *42*, 7881−7888.

(13) Ghanem, B. S.; McKeown, N. B.; Budd, P. M.; Selbie, J. D.; Fritsch, D. *Adv. Mater.* **2008**, *20*, 2766−2771.

(14) Du, N. Y.; Park, H. B.; Robertson, G. P.; Dal-Cin, M. M.; Visser, T.; Scoles, L.; Guiver, M. D. *Nat. Mater.* **2011**, *10*, 372−375.

(15) Du, N. Y.; Dal-Cin, M. M.; Robertson, G. P.; Guiver, M. D. *Macromolecules* **2012**, *45*, 5134−5139.

(16) Du, N. Y.; Robertson, G. P.; Pinnau, I.; Guiver, M. D. *Macromolecules* **2010**, *43*, 8580−8587.

(17) Du, N. Y.; Robertson, G. P.; Pinnau, I.; Guiver, M. D. *Macromolecules* **2009**, *42*, 6023−6030.

(18) Du, N. Y.; Robertson, G. P.; Song, J. S.; Pinnau, I.; Thomas, S.; Guiver, M. D. *Macromolecules* **2008**, *41*, 9656−9662.

(19) Maier, G. *Angew. Chem., Int. Ed.* **2013**, *52*, 4982−4984.

(20) Park, H. B.; Jung, C. H.; Lee, Y. M.; Hill, A. J.; Pas, S. J.; Mudie, S. T.; Van Wagner, E.; Freeman, B. D.; Cookson, D. J. *Science* **2007**, *318*, 254−258.

(21) Ma, X. H.; Swaidan, R.; Belmabkhout, Y.; Zhu, Y. H.; Litwiller, E.; Jouiad, M.; Pinnau, I.; Han, Y. *Macromolecules* **2012**, *45*, 3841−3849.

(22) Ghanem, B. S.; Swaidan, R.; Litwiller, E.; Pinnau, I. *Adv. Mater.* **2014**, DOI: 10.1002/adma.201306229.

(23) Rogan, Y.; Starannikova, L.; Ryzhikh, V.; Yampolskii, Y.; Bernardo, P.; Bazzarelli, F.; Jansen, J. C.; McKeown, N. B. *Polym. Chem.* **2013**, *4*, 3813−3820.

(24) Rogan, Y.; Malpass-Evans, R.; Carta, M.; Lee, M.; Jansen, J. C.; Bernardo, P.; Clarizia, G.; Tocci, E.; Friess, K.; Lanc, M.; McKeown, N. B. *J. Mater. Chem. A* **2014**, *2*, 4874−4877.

(25) Baker, R. W. *Ind. Eng. Chem. Res.* **2002**, *41*, 1393−1411.

(26) Guiver, M. D.; Lee, Y. M. *Science* **2013**, *339*, 284−285.

(27) Ghanem, B. S.; McKeown, N. B.; Budd, P. M.; Fritsch, D. *Macromolecules* **2008**, *41*, 1640−1646.

(28) Heuchel, M.; Fritsch, D.; Budd, P. M.; McKeown, N. B.; Hofmann, D. *J. Membr. Sci.* **2008**, *318*, 84−99.

(29) Robeson, L. M. *J. Membr. Sci.* **2008**, *320*, 390−400.

(30) O'Brien, K. C.; Koros, W. J.; Barbari, T. A.; Sanders, E. S. *J. Membr. Sci.* **1986**, *29*, 229−238.

(31) Sydlik, S. A.; Chen, Z. H.; Swager, T. M. *Macromolecules* **2011**, *44*, 976−980.

(32) Cho, Y. J.; Park, H. B. *Macromol. Rapid Commun.* **2011**, *32*, 579−586.

(33) Mao, H. C.; Zhang, S. *Polymer* **2014**, *55*, 102−109.

(34) Ritter, N.; Senkovska, I.; Kaskel, S.; Weber, J. *Macromolecules* **2011**, *44*, 2025−2033.

(35) Li, S.; Jo, H. J.; Han, S. H.; Park, C. H.; Kim, S.; Budd, P. M.; Lee, Y. M. *J. Membr. Sci.* **2013**, *434*, 137−147.

(36) Du, N. Y.; Song, J. S.; Robertson, G. P.; Pinnau, I.; Guiver, M. D. *Macromol. Rapid Commun.* **2008**, *29*, 783−788.

(37) Masuda, T.; Tang, B. Z.; Tanaka, A.; Higashimura, T. *Macromolecules* **1986**, *19*, 1459−1464.

(38) Zhou, J.; Zhu, X.; Hu, J.; Liu, H.; Hu, Y.; Jiang, J. *Phys. Chem. Chem. Phys.* **2014**, *16*, 6075−6083.

(39) Morisato, A.; Shen, H. C.; Sankar, S. S.; Freeman, B. D.; Pinnau, I.; Casillas, C. G. *J. Polym. Sci., Polym. Phys.* **1996**, *34*, 2209−2222.

(40) Merkel, T. C.; Freeman, B. D.; Spontak, R. J.; He, Z.; Pinnau, I.; Meakin, P.; Hill, A. J. *Science* **2002**, *296*, 519−522.

(41) Pinnau, I.; Casillas, C. G.; Morisato, A.; Freeman, B. D. *J. Polym. Sci., Polym. Phys.* **1996**, *34*, 2613−2621.

(42) Thomas, S.; Pinnau, I.; Du, N. Y.; Guiver, M. D. *J. Membr. Sci.* **2009**, *333*, 125−131.

(43) Thomas, S.; Pinnau, I.; Du, N. Y.; Guiver, M. D. *J. Membr. Sci.* **2009**, *338*, 1−4.

(44) Hofmann, D.; Ulbrich, J.; Fritsch, D.; Paul, D. *Polymer* **1996**, *37*, 4773−4785.

(45) Stern, S. A.; Mi, Y.; Yamamoto, H.; St. Clair, A. K. *J. Polym. Sci., Polym. Phys.* **1989**, *27*, 1887−1909.

(46) Kim, T. H.; Koros, W. J.; Husk, G. R.; O'Brien, K. C. *J. Membr. Sci.* **1988**, *37*, 45−62.

(47) Tanaka, K.; Okano, M.; Toshino, H.; Kita, H.; Okamoto, K. I. *J. Polym. Sci., Polym. Phys.* **1992**, *30*, 907−914.

(48) Tanaka, K.; Kita, H.; Okano, M.; Okamoto, K. *Polymer* **1992**, *33*, 585−592.

(49) Tanaka, K.; Okamoto, K.-I. Structure and Transport Properties of Polyimides as Materials for Gas and Vapor Membrane Separation. In *Materials Science of Membranes for Gas and Vapor Separation*; John Wiley & Sons, Ltd.: New York, 2006; pp 271−291.

(50) Pinnau, I.; Morisato, A.; He, Z. J. *Macromolecules* **2004**, *37*, 2823−2828.

(51) Pinnau, I.; He, Z. J.; Morisato, A. *J. Membr. Sci.* **2004**, *241*, 363−369.

(52) Staiger, C. L.; Pas, S. J.; Hill, A. J.; Cornelius, C. J. *Chem. Mater.* **2008**, *20*, 2606−2608.

(53) Budd, P. M.; McKeown, N. B.; Ghanem, B. S.; Msayib, K. J.; Fritsch, D.; Starannikova, L.; Belov, N.; Sanfirova, O.; Yampolskii, Y.; Shantarovich, V. *J. Membr. Sci.* **2008**, *325*, 851−860.